Published in final edited form as:
Nucl Med Biol. 2013 October ; 40(7): 906–911. doi:10.1016/j.nucmedbio.2013.06.008.

Imaging of Carrageenan-Induced Local Inflammation and Adjuvant-Induced Systemic Arthritis with [^{11}C]PBR28 PET

Xia Shao[1], **Xueding Wang**[1], **Sean J English**[2], **Timothy Desmond**[1], **Phillip S Sherman**[1], **Carole A Quesada**[1], and **Morand R Piert**[1]

[1]Department of Radiology, University of Michigan Health System, Ann Arbor, MI, USA

[2]Conrad Jobst Vascular Research Laboratory, Department of Surgery, University of Michigan Health System, Ann Arbor, MI, USA

Abstract

Introduction—[^{11}C]PBR28 binding to translocator protein (TSPO) was evaluated for imaging of acute and chronic inflammation using two established rat models.

Methods—Acute inflammation was induced by local Carrageenan-injection into the paw of Fisher 344 rats (model A). T-cell mediated adjuvant arthritis was induced by heat-inactivated Mycobacterium butyricum injection in Lewis rats (model B). Micro-PET scan was performed after injection of approximately 35 MBq [^{11}C]PBR28. In model A, volumes of interest (VOIs) were defined in the paw of Fisher 344 rats (n=6) with contralateral sham treatment as control. For model B, VOIs were defined in the tail, sacroiliac joints, hips, knees and thigh muscles of M. butyricum treated animals (n=8) and compared with sham-treated controls (n=4). The peak ^{11}C-PBR28 SUV (SUV_{peak}) and area under the curve (AUC_{SUV}) of 60-minute time-activity data were calculated. Immunohistochemistry for CD68, a macrophage stain, was performed from paw tissues. In addition, the [^{11}C]PBR28 cell uptake was measured in lipopolysaccharide (LPS)-stimulated and non-stimulated macrophage cultures.

Results—LPS-stimulated macrophages displayed dose-dependent increased [^{11}C]PBR28 uptake, which was blocked by non-labeled PBR28. In both models, radiotracer uptake of treated lesions increased rapidly within minutes and displayed overall accumulative kinetics. The SUV_{peak} and AUC_{SUV} of Carrageenan-treated paws was significantly increased compared to controls. Also, the [^{11}C]PBR28 uptake ratio of Carrageenan-treated vs. sham-treated paw correlated significantly with CD68 staining ratios of the same animals. In adjuvant arthritis, significantly increased [^{11}C]PBR28 SUV_{peak} and AUC_{SUV} values were identified at the tail, knees, and sacroiliac joints, while no significant differences were identified in the lumbar spine and hips.

Conclusions—Based on our initial data, [^{11}C]PBR28 PET appears to have potential for imaging of various inflammatory processes involving macrophage activation.

Correspondence: Morand Piert, M.D., University of Michigan Health System, Department of Radiology, Division of Nuclear Medicine, University Hospital B1G505C, 1500 E. Medical Center Drive, Ann Arbor, MI 48109-0028, mpiert@med.umich.edu, Tel.: +1 7349365388, Fax: +1 7349368182.

Competing interests
The authors declare that they have no competing interests.

Keywords

[^{11}C]PBR28; TSPO; systemic adjuvant arthritis; Carrageenan-induced inflammation; macrophages; RAW 264.7 cells

BACKGROUND

The 18kDa translocator protein TP-18 (TSPO), earlier called peripheral benzodiazepine receptor (PBR), is a five transmembrane domain protein associated with many biological processes. High TSPO protein levels are found in steroid-synthesizing tissues, secretory and glandular tissues and olfactory epithelium, intermediate levels in renal and myocardial tissues, and low levels in the brain and liver [1]. TSPO is involved in a variety of cellular functions, most notably cholesterol transport and steroid hormone synthesis, mitochondrial respiration, mitochondrial permeability transition pore (MPTP) opening, apoptosis, and cell proliferation [2, 3]. TSPO is mainly situated in the outer mitochondrial membrane, but has been found in lysosomes, peroxisomes, nucleus, plasma membrane, and mature human red cells [1, 3].

Currently, TSPO is actively been investigated as a marker of reactive gliosis and inflammation associated with a variety of neuropathological conditions [4, 5]. Upon activation microglia express binding sites for ligands recognizing TSPO. A number of PET radiotracers have been developed to study binding to TSPO as surrogate markers of neuro-inflammation with [^{11}C](*R*)-PK11195 being the prototype molecule. Limitations of [^{11}C](*R*)-PK11195 such as poor bioavailability in brain tissue and non-specific binding causing inadequate signal-to-noise ratios led to the development of other second generation TSPO ligands such as [^{11}C]PBR28 [6], a PET radiotracer with improved biodistribution [7], which was used in this study.

More recently, TSPO overexpression has been linked to the activation of the immunological response to inflammation in arterial plaques [8–10], rheumatoid synovitis [11], and osteoarthritis [12]. In addition, TSPO-tracers may have utility for PET imaging of glioma [13, 14]. Here, we present first pilot data evaluating the potential of [^{11}C]PBR28 for PET imaging of extra-cranial inflammation. In this study, we used two well established rat models of acute inflammation and adjuvant arthritis. Acute inflammation was induced by Carrageenan injection into the hind paws [15]. Systemic T-cell mediated autoimmune (adjuvant) arthritis, which has similarities to rheumatoid arthritis, was induced by injection of heat-inactivated Mycobacterium butyricum [16].

METHODS

Radiotracer Synthesis

[^{11}C]PBR28 was synthesized using modified GE Tracerlab FX C Pro based on the method of Shao et al. [17]. Briefly, the precursor, desmethyl-PBR28 TBA salt (1 mg) was dissolved into absolute ethanol (100 μL), loaded onto the 2 mL stainless steel HPLC loop, and conditioned with nitrogen gas for 20 seconds at 10 mL/min. [^{11}C]MeOTf was prepared according to the general procedure [18] and passed through the HPLC loop at 12 mL/min for 5 minutes. Following reaction, the mixture was purified by semi-preparative HPLC (column: Prodigy ODS 250 × 10 mm, mobile phase: 40% CH_3CN, flow rate: 5 mL/min). The radioactive product peak was collected (retention time ~12 min) into 50 mL of water and then passed through a C-18 extraction cartridge. The cartridge was washed with 7 mL USP water. The final product was eluted with 0.5 mL of USP ethanol, followed by 9.5 mL of USP saline for injection. This aqueous solution was filtered through a 0.22 μm sterile filter

into a sterile dose vial and submitted for QC testing. Quality control analyses were performed based on the standard operation procedures of routine clinical production [19].

Animal Models

The animal research protocol was performed in compliance with internationally recognized principles of laboratory animal care and was approved by the University of Michigan Committee on Use and Care of Animals (protocol numbers 9088 and 9927). For all procedures, animals were anesthetized using an isoflurane-oxygen mix (5% isofluorane for induction and 1–2% for maintenance).

Carrageenan-Induced Paw Edema in the Rat (Model A)—The Carrageenan-induced hind paw edema model has extensively been used as a model of acute inflammation [15]. Six Fisher 344 rats (Charles-River) were injected with 0.1 ml of 1% carrageenan solution (Sigma) using a 30-gauge hypodermic needle. The needle was inserted into the pad region of the glabrous skin and moved 6 to 8 mm proximal towards the tarsal region. The contralateral paws were injected with 0.1 ml of saline as control. PET imaging was performed at the time of maximum local edema (3 hours after treatment) [20].

Adjuvant Arthritis Model (Model B)—A systemic T-cell mediated autoimmune arthritis was induced in 8 genetically susceptible female Lewis rats (~ 100 g body weight) by subcutaneous injection into the base of the tail with lyophilized (inactivated) Mycobacterium butyricum (0.3 ml; Difco, Detroit, Michigan) suspended in mineral oil at 5 mg/ml [21]. Articular index scores (0 = no swelling or erythema, 1 = slight swelling and/or erythema, 2 = low-to-moderate edema, 3 = pronounced edema with limited use of the joint, and 4 = excessive edema with joint rigidity) were recorded for tail joints and knees as described in the literature [22]. Around 20 days after treatment, adjuvant arthritis animals showed a steep increase in clinical scores from 0 to 3–4 for the tail and knees. Four sham-treated animals (saline injection) served as controls. Their articular index scores were 0 for knees and tail. PET imaging was performed 3–4 weeks after treatment.

PET Imaging and Data Analysis

Animals were placed prone within a microPET scanner (R4 or P4, Siemens/Concorde Microsystems, Inc., Knoxville, TN, USA) [23]. Body temperature, maintained using a circulating water warming pad, and respiratory rate were monitored during imaging. Following a measured transmission scan, dynamic PET was performed for 60 minutes (10 × 30 sec, 3 × 1 min, 1 × 2 min, 4 × 5 min, 3 × 10 min). For model A experiments, the field of view included the hind limbs, while in model B abdomen, pelvis, proximal lower extremities and knees were included. With the start of the dynamic sequence, ~ 35 MBq (equaling ~ 5 nmol) of [^{11}C]PBR28 (in 0.2 ml) was injected intravenously into a tail vein followed by a 1 ml flush of saline.

After correction for decay, dead time and random coincidences, data were reconstructed using iterative ordered subset expectation maximization – maximum a posteriori (OSEM-MAP) [24] yielding a reconstructed image resolution of approximately 1.4 mm on both scanners. Regions of interest (ROIs) were defined using standardized rectangular ROIs measuring 5 × 3 pixels placed on the image slice with the maximum uptake in the target regions (muscle, lumbar spine, root of tail, as well as hip, knee, and sarcroiliac joints), thereby determining the peak standardized uptake value (SUV_{peak}) [25] of data obtained between 30–60 minutes using ASI Pro VM software (Siemens Medical Systems, Malvern, PA). For model A experiments, Carrageenan-to-control ratios were calculated for further analysis. Sigma Plot (Systat, Chicago, IL) was used to calculate the area under the curve for

normalized mean SUV time activity data (AUC_{SUV}) between 0 and 60 minutes post tracer injection.

Histology and Immunohistochemistry

Tissue from both paws of 5 Fisher 344 rats (model A) were available for histologic analysis using a macrophage stain performed with a mouse anti-rat CD68 primary antibody (1:67) Serotec, Raleigh, NC) [26]. Utilizing a Leica DMR microscope (Leica Microsystems IN, Buffalo Grove, IL), motorized stage, and Stereo Investigator software (Version 4.34, Microbrightfield Inc., Williston, VT) stereologic assessments (average of 140 high-power fields at 63×) of control and carrageenan-treated sections were evaluated [27]. Macrophage and muscle estimates per unit area (μm^2) were determined and tissue-to-muscle and Carrageenan-to-vehicle ratios were determined for each animal. Histological evaluation was performed by an experienced reader blinded to imaging results.

Macrophage Cell Culture Experiments

To test [^{11}C]PBR28 uptake in response to stimulation of macrophages, the murine RAW 264.7 macrophage cell line was obtained (Sigma) and maintained in complete RPMI 1640 (C-RPMI), which contains 1140 mmol/L L-Arg (BioWhitaker Walkersville, MD) and supplemented with 10% fetal calf serum, 25 mmol/L HEPES, 4 mmol/L L-glutamine, and 100 units/mL penicillin/streptomycin. The cells were grown to approximately 80% confluence on polystyrene 6-well plates in C-RPMI. [^{11}C]PBR28 cell uptake was determined in macrophages stimulated at 10, 100 and 1000 μg/ml lipopolysaccharide (LPS, Sigma) for 24 h and compared to non-stimulated cultures. Samples were incubated for 10 minutes with ~0.6 MBq of [^{11}C]PBR28 (at ~0.05 pmol/mL concentration). Non-specific binding was determined in parallel blocking experiments were samples were incubated with excess amounts of cold PBR28 (480 pmol/mL) for 30 minutes prior to adding [^{11}C]PBR28. Cell numbers per sample were determined greater than 25 million for each level. Cells were washed 3 times in ice-cold PBS before counting. All experiments were performed in triplicate.

Statistics

Parameters were compared by means of a one-way ANOVA, including tests for homogeneity of group variances using the Bartlett test, selecting a conservative significance level of $P \geq 0.1$. In case of homogenous group variances, the data were then compared using a *t*-test, otherwise a Wilcoxon rank-sign test was applied. Results are expressed as mean ± SD. $P < 0.05$ was considered statistically significant. Statistical tests were performed with the JMP (SAS) statistical software package.

RESULTS

Biodistribution

The radiotracer showed avid uptake in the liver with biliary excretion of radioactivity into bowel as well as fast renal excretion and subsequent accumulation of radioactivity in the bladder. Additional radiotracer accumulation was noted in visualized bones and spleen. The SUV_{peak} of [^{11}C]PBR28 of untreated animals of both rat species was significantly higher in bone than compared to muscle ($p < 0.001$), suggesting binding of [^{11}C]PBR28 to TSPO-positive bone and/or marrow cells.

Carrageenan Model

Radiotracer uptake in 5 out of 6 Carrageenan-treated paws was visually increased compared to the contralateral side, while in one experiment radiotracer uptake of the treated side was

similar to the control side. A representative case is demonstrated in Figure 1. The [^{11}C]PBR28 SUV_{peak} was significantly higher in Carrageenan-treated paws compared to paired contralateral controls (SUV_{peak} 1.02 ± 0.27 vs. 0.72 ± 0.34; paired *t*-test $p < 0.01$), while no significant difference was seen in thigh muscles. Figure 2 shows time-activity data (same case as Figure 1) with accumulative tracer kinetics. Also, the mean AUC_{SUV} of Carrageenan-treated paws was significantly increased compared to contralateral controls (AUC_{SUV}: 3040.9 ± 1182.3 vs. 2028.0 ± 1123.4, paired *t*-test $p < 0.05$), respectively. As can be seen from the AUC_{SUV} of thigh muscles, Carrageenan-treatment did not increase thigh muscle uptake on either side (Carrageenan-treated side: 764.9 ± 318.5 vs. controls 776.2 ± 354.9).

Adjuvant Arthritis Model

The results are summarized in Table 1. Time-activity data showed rapid tracer uptake and accumulative kinetics in adjuvant arthritis with minimal accumulation of radioactivity in control tissues. Figure 3 illustrates this behavior for adjuvant arthritis in the root of the tail compared to sham treatment.

Increased [^{11}C]PBR28 uptake (SUV_{peak}) was identified at the root of the tail (Figure 4), sacroiliac joints and knees, while no significant differences were identified in the lumbar spine and hips. Also, the mean AUC_{SUV} of the root of the tail, knees and sacroiliac joints was significantly increased compared to control animals, while no such difference was noted for the lumbar spine and hips. The AUC_{SUV} of thigh muscle was not affected by inducing adjuvant arthritis. However, the SUV_{peak} and AUC_{SUV} of muscle was significantly lower than any other measured tissue.

Histology and Immunohistochemistry

Stereologic assessments revealed positive staining in Carrageenan-treated paws compared to control paws of the same animal. On average 1845 cells were counted positive on the Carrageenan-treated side vs. 570 on the contralateral side assessing the entire paw surface area (mean 24.2 mm^2 per side). However 3 hours after Carrageenan injection, the overall density of CD68-positive cells was low. Nevertheless, Carrageenan-treated tissue displayed on average a 1.8-fold increase of CD68 positive cells per μmm^2. A representative case is shown in Figure 5.

Also, [^{11}C]PBR28 uptake was related to the number of CD68 positive macrophages. The [^{11}C]PBR28 SUV_{peak} ratios (Carrageenan-treated over controls) correlated significantly with the CD68 staining ratios of the 5 animals available for analysis (see supplemental data: Figure 6). Interestingly, the animal without perceivable Carrageenan-induced changes on PET also showed a lack of increased CD68 staining on the treated side.

Macrophage cell culture experiments

Stimulation of macrophages with LPS resulted in a dose-dependent increased [^{11}C]PBR28 uptake compared to non-stimulated macrophages. Uptake was significantly blocked by excess non-labeled PBR28 at any stimulation-level, indicating specificity of [^{11}C]PBR28 for TSPO (Figure 7).

DISCUSSION

PET imaging of arthritis has been suggested to determine the severity and extend of disease and to assess response to treatment. However, while assessing metabolic changes in arthritis with ^{18}F-FDG PET is widely available, clinical applications are rare [28, 29]. As a metabolic marker, ^{18}F-FDG lacks true specificity for inflammatory processes. Therefore,

radiotracers that would be able to specifically assess the inflammatory burden of disease are needed. To test the hypothesis that TSPO-binding radiotracers could be used for in vivo imaging of rheumatoid synovitis, Van der Laken et al. investigated [^{11}C](*R*)-PK11195 in patients with rheumatoid arthritis [11]. They concluded that [^{11}C](*R*)-PK11195 PET is useful for both, early detection of synovitis and monitoring of disease activity during treatment.

Here we tested [^{11}C]PBR28, a second generation PET radiotracer for imaging of TSPO binding with improved signal-to-noise ratios compared to [^{11}C](*R*)-PK11195 [7], in macrophage cell cultures and two well-established rat models of acute inflammation and adjuvant-induced arthritis. The study demonstrates for the first time that [^{11}C]PBR28 can visualize the inflammatory response typically seen in both models.

Macrophage cell culture experiments indicated a dose-dependent increase of [^{11}C]PBR28 uptake with the level of LPS stimulation. These data are in agreement with earlier in-vitro macrophage studies using labeled PK11195 [10] and indicate that the uptake of TSPO-binding radiotracers increases upon activation of macrophages. Furthermore, our blocking experiments indicated specificity of [^{11}C]PBR28 uptake for TSPO in both, non-stimulated and LPS stimulated macrophages. In addition, the level of [^{11}C]PBR28 uptake in Carrageenan-treated paw tissues correlated with increased macrophage-specific CD68 protein staining. Similarily, other investigators verified spatial co-localization of CD68 staining and [^{3}H]PK11195 uptake on autoradiography [8, 9]. These data indicate the potential of TSPO ligands for PET imaging of macrophage-rich tissues or tissues with a significant population of activated macrophages.

The adjuvant-induced arthritis rat model is clinically and pathologically similar to rheumatoid arthritis [30–32]. It is well known that synovial lining cells that normally enclose the joint cavity proliferate during the course of inflammatory diseases such as rheumatoid arthritis and osteoarthritis [33]. The role of activated macrophages in the pathogenesis of this model has been extensively investigated [34–36]. Upregulation of TSPO has been identified in adjuvant-induced arthritis and autoimmune encephalomyelitis [37, 38]. In adjuvant arthritis, we identified increased [^{11}C]PBR28 uptake in several joints, indicating its clinical potential. While the use of adjuvant-induced inflammation to study TSPO-binding radiotracers has been applied to study brain inflammation [38], application of [^{11}C]PBR28 to study adjuvant-induced inflammation outside of the brain has not been performed.

The Carrageenan-induced inflammation in the rat paw model has been extensively used in the development of non-steroidal anti-inflammatory drugs and selective cyclooxygenase 1 and 2 inhibitors [15, 39]. The maximum of the acute inflammatory response to Carrageenan is typically seen around 3 hours after injection. In this model, several TSPO ligands including PK11195 have demonstrated TSPO-mediated anti-edamatogenic and antinociceptive effects when given in pharmacological doses [40]. Also, diazepam reduces the Carrageenan-induced inflammatory paw edema in rats via action on TSPO receptors [41, 42]. Our results indicated increased [^{11}C]PBR28 uptake 3 hours after Carrageenan-induced acute paw edema. As acute inflammation will increase local blood flow and vascular permeability [43], increased [^{11}C]PBR28 is expected simply due to locally increased perfusion. In addition, we suspect that besides perfusion-related changes, migration of activated macrophages into the affected paw tissue may play a role as well. First, we identified accumulative tracer kinetics which cannot be simply explained by increased perfusion (as this would result in a flat, plateau-type uptake curve). Furthermore, the correlation between CD68 stains and [^{11}C]PBR28 uptake measures suggests that migration of TSPO-expressing macrophages into the Carrageenan-treated tissues may have contributed

to the observed increased [^{11}C]PBR28 uptake. As identified in our cell culture experiments, the number of macrophages seen in inflammation as well as their level of activation influences [^{11}C]PBR28 uptake.

We identified increased [^{11}C]PBR28 uptake in the bone and bone marrow, which was significantly higher than muscle background in treated and untreated animals. These findings can be explained by recent research indicating that TSPO expression is found in bone marrow and trabecular bone, particularly in osteoblasts and osteoclasts [44]. As a result, the physiologic uptake of [^{11}C]PBR28 in bone may actually have lessened our ability to identify additional inflammation-induced TSPO expression as inflamed joints are located close to bone and overlap of VOIs with bone may have occurred.

Conclusion

While many aspects of TSPO expression in acute inflammation and adjuvant arthritis are still unknown, our pilot data suggest that [^{11}C]PBR28 appears to be a promising radiotracer for PET imaging of various inflammatory processes involving macrophage activation.

Supplementary Material

Refer to Web version on PubMed Central for supplementary material.

Acknowledgments

Supported by the National Institutes of Health (NIH) under grant number R01 AR060350 and R01 AR055179.

REFERENCES

1. Batarseh A, Papadopoulos V. Regulation of translocator protein 18 kDa (TSPO) expression in health and disease states. Mol Cell Endocrinol. 2010; 327:1–12. [PubMed: 20600583]
2. Veenman L, Gavish M. The role of 18 kDa mitochondrial translocator protein (TSPO) in programmed cell death, and effects of steroids on TSPO expression. Curr Mol Med. 2012; 12:398–412. [PubMed: 22348610]
3. Rupprecht R, Papadopoulos V, Rammes G, Baghai TC, Fan J, Akula N, et al. Translocator protein (18 kDa) (TSPO) as a therapeutic target for neurological and psychiatric disorders. Nat Rev Drug Discov. 2010; 9:971–988. [PubMed: 21119734]
4. Chen MK, Guilarte TR. Translocator protein 18 kDa (TSPO): molecular sensor of brain injury and repair. Pharmacol Ther. 2008; 118:1–17. [PubMed: 18374421]
5. Papadopoulos V, Lecanu L. Translocator protein (18 kDa) TSPO: an emerging therapeutic target in neurotrauma. Exp Neurol. 2009; 219:53–57. [PubMed: 19409385]
6. Bartels AL, Willemsen AT, Doorduin J, de Vries EF, Dierckx RA, Leenders KL. [11C]-PK11195 PET: quantification of neuroinflammation and a monitor of anti-inflammatory treatment in Parkinson's disease? Parkinsonism Relat Disord. 2010; 16:57–59. [PubMed: 19487152]
7. Chauveau F, Boutin H, Van Camp N, Dolle F, Tavitian B. Nuclear imaging of neuroinflammation: a comprehensive review of [11C]PK11195 challengers. Eur J Nucl Med Mol Imaging. 2008; 35:2304–2319. [PubMed: 18828015]
8. Fujimura Y, Hwang PM, Trout Iii H, Kozloff L, Imaizumi M, Innis RB, et al. Increased peripheral benzodiazepine receptors in arterial plaque of patients with atherosclerosis: an autoradiographic study with [(3)H]PK 11195. Atherosclerosis. 2008; 201:108–111. [PubMed: 18433754]
9. Gaemperli O, Shalhoub J, Owen DR, Lamare F, Johansson S, Fouladi N, et al. Imaging intraplaque inflammation in carotid atherosclerosis with 11C-PK11195 positron emission tomography/computed tomography. Eur Heart J. 2012; 33:1902–1910. [PubMed: 21933781]

10. Bird JL, Izquierdo-Garcia D, Davies JR, Rudd JH, Probst KC, Figg N, et al. Evaluation of translocator protein quantification as a tool for characterising macrophage burden in human carotid atherosclerosis. Atherosclerosis. 2010; 210:388–391. [PubMed: 20056222]
11. van der Laken CJ, Elzinga EH, Kropholler MA, Molthoff CF, van der Heijden JW, Maruyama K, et al. Noninvasive imaging of macrophages in rheumatoid synovitis using 11C-(R)-PK11195 and positron emission tomography. Arthritis Rheum. 2008; 58:3350–3355. [PubMed: 18975347]
12. Giusti L, Betti L, Giannaccini G, Mascia G, Bazzichi L, Lucacchini A. [3H]PK11195 binding sites in human neutrophils: effect of fMLP stimulation and modulation in rheumatic diseases. Clin Biochem. 2004; 37:61–66. [PubMed: 14675564]
13. Winkeler A, Boisgard R, Awde AR, Dubois A, Theze B, Zheng J, et al. The translocator protein ligand [(1)(8)F]DPA-714 images glioma and activated microglia in vivo. Eur J Nucl Med Mol Imaging. 2012; 39:811–823. [PubMed: 22270507]
14. Tang D, Hight MR, McKinley ET, Fu A, Buck JR, Smith RA, et al. Quantitative preclinical imaging of TSPO expression in glioma using N,N-diethyl-2-(2-(4-(2-18F-fluoroethoxy)phenyl)-5,7-dimethylpyrazolo[1,5-a]pyrimi din-3-yl)acetamide. J Nucl Med. 2012; 53:287–294. [PubMed: 22251555]
15. Morris CJ. Carrageenan-induced paw edema in the rat and mouse. Methods Mol Biol. 2003; 225:115–121. [PubMed: 12769480]
16. Feketeova L, Jancova P, Moravcova P, Janegova A, Bauerova K, Ponist S, et al. Effect of methotrexate on inflammatory cells redistribution in experimental adjuvant arthritis. Rheumatol Int. 2011
17. Hoareau R, Shao X, Henderson BD, Scott PJ. Fully automated radiosynthesis of [(11)C]PBR28, a radiopharmaceutical for the translocator protein (TSPO) 18kDa, using a GE TRACERlab FX(C-Pro). Appl Radiat Isot. 2012
18. Shao X, Kilbourn MR. A simple modification of GE tracerlab FX C Pro for rapid sequential preparation of [11C]carfentanil and [11C]raclopride. Appl Radiat Isot. 2009; 67:602–605. [PubMed: 19162491]
19. Shao X, Hoareau R, Hockley BG, Tluczek LJ, Henderson BD, Padgett HC, et al. Highlighting the Versatility of the Tracerlab Synthesis Modules. Part 1: Fully Automated Production of [F]Labelled Radiopharmaceuticals using a Tracerlab FX(FN). J Labelled Comp Radiopharm. 2011; 54:292–307. [PubMed: 21769163]
20. Otterness IG, Moore PF. Carrageenan foot edema test. Methods Enzymol. 1988; 162:320–327. [PubMed: 3226312]
21. Halloran MM, Szekanecz Z, Barquin N, Haines GK, Koch AE. Cellular adhesion molecules in rat adjuvant arthritis. Arthritis Rheum. 1996; 39:810–819. [PubMed: 8639178]
22. Wang CR, Chen SY, Wu CL, Liu MF, Jin YT, Chao L, et al. Prophylactic adenovirus-mediated human kallistatin gene therapy suppresses rat arthritis by inhibiting angiogenesis and inflammation. Arthritis Rheum. 2005; 52:1319–1324. [PubMed: 15818689]
23. Knoess C, Siegel S, Smith A, Newport D, Richerzhagen N, Winkeler A, et al. Performance evaluation of the microPET R4 PET scanner for rodents. Eur J Nucl Med Mol Imaging. 2003; 30:737–747. [PubMed: 12536244]
24. Bai B, Li Q, Holdsworth CH, Asma E, Tai YC, Chatziioannou A, et al. Model-based normalization for iterative 3D PET image reconstruction. Phys Med Biol. 2002; 47:2773–2784. [PubMed: 12200938]
25. Benz MR, Czernin J, Allen-Auerbach MS, Tap WD, Dry SM, Elashoff D, et al. FDG-PET/CT imaging predicts histopathologic treatment responses after the initial cycle of neoadjuvant chemotherapy in high-grade soft-tissue sarcomas. Clin Cancer Res. 2009; 15:2856–2863. [PubMed: 19351756]
26. Cho BS, Woodrum DT, Roelofs KJ, Stanley JC, Henke PK, Upchurch GR Jr. Differential regulation of aortic growth in male and female rodents is associated with AAA development. J Surg Res. 2009; 155:330–338. [PubMed: 19111327]
27. West MJ, Slomianka L, Gundersen HJ. Unbiased stereological estimation of the total number of neurons in thesubdivisions of the rat hippocampus using the optical fractionator. Anat Rec. 1991; 231:482–497. [PubMed: 1793176]

28. Beckers C, Ribbens C, Andre B, Marcelis S, Kaye O, Mathy L, et al. Assessment of disease activity in rheumatoid arthritis with (18)F-FDG PET. J Nucl Med. 2004; 45:956–964. [PubMed: 15181130]
29. Roivainen A, Parkkola R, Yli-Kerttula T, Lehikoinen P, Viljanen T, Mottonen T, et al. Use of positron emission tomography with methyl-11C-choline and 2-18F-fluoro-2-deoxy-D-glucose in comparison with magnetic resonance imaging for the assessment of inflammatory proliferation of synovium. Arthritis Rheum. 2003; 48:3077–3084. [PubMed: 14613269]
30. Wooley PH. Animal models of rheumatoid arthritis. Curr Opin Rheumatol. 1991; 3:407–420. [PubMed: 1909156]
31. Halloran MM, Woods JM, Strieter RM, Szekanecz Z, Volin MV, Hosaka S, et al. The role of an epithelial neutrophil-activating peptide-78-like protein in rat adjuvant-induced arthritis. J Immunol. 1999; 162:7492–7500. [PubMed: 10358204]
32. Shahrara S, Proudfoot AE, Woods JM, Ruth JH, Amin MA, Park CC, et al. Amelioration of rat adjuvant-induced arthritis by Met-RANTES. Arthritis Rheum. 2005; 52:1907–1919. [PubMed: 15934086]
33. Kamimoto M, Kikuchi M, Yashiro T, Nihe A, Kariya Y, Hoshino Y. Immunohistochemical study of the proliferation modality of synovium in rat adjuvant arthritis. J Orthop Sci. 2003; 8:400–407. [PubMed: 12768485]
34. Turk MJ, Breur GJ, Widmer WR, Paulos CM, Xu LC, Grote LA, et al. Folate-targeted imaging of activated macrophages in rats with adjuvant-induced arthritis. Arthritis Rheum. 2002; 46:1947–1955. [PubMed: 12124880]
35. Haas CS, Martinez RJ, Attia N, Haines GK 3rd, Campbell PL, Koch AE. Chemokine receptor expression in rat adjuvant-induced arthritis. Arthritis Rheum. 2005; 52:3718–3730. [PubMed: 16320322]
36. Johnson WJ, Muirhead KA, Meunier PC, Votta BJ, Schmitt TC, DiMartino MJ, et al. Macrophage activation in rat models of inflammation and arthritis. Systemic activation precedes arthritis induction and progression. Arthritis Rheum. 1986; 29:1122–1130. [PubMed: 3489469]
37. Hernstadt H, Wang S, Lim G, Mao J. Spinal translocator protein (TSPO) modulates pain behavior in rats with CFA-induced monoarthritis. Brain res. 2009; 1286:42–52. [PubMed: 19555675]
38. Mattner F, Katsifis A, Staykova M, Ballantyne P, Willenborg DO. Evaluation of a radiolabelled peripheral benzodiazepine receptor ligand in the central nervous system inflammation of experimental autoimmune encephalomyelitis: a possible probe for imaging multiple sclerosis. Eur J Nucl Med Mol Imaging. 2005; 32:557–563. [PubMed: 15875181]
39. Guay J, Bateman K, Gordon R, Mancini J, Riendeau D. Carrageenan-induced paw edema in rat elicits a predominant prostaglandin E2 (PGE2) response in the central nervous system associated with the induction of microsomal PGE2 synthase-1. J Biol Chem. 2004; 279:24866–24872. [PubMed: 15044444]
40. Bressan E, Farges RC, Ferrara P, Tonussi CR. Comparison of two PBR ligands with classical antiinflammatory drugs in LPS-induced arthritis in rats. Life sci. 2003; 72:2591–2601. [PubMed: 12672505]
41. Lazzarini R, Maiorka PC, Liu J, Papadopoulos V, Palermo-Neto J. Diazepam effects on carrageenan-induced inflammatory paw edema in rats: role of nitric oxide. Life sci. 2006; 78:3027–3034. [PubMed: 16438989]
42. Lazzarini R, Sakai M, Costa-Pinto FA, Palermo-Neto J. Diazepam decreases leukocyte-endothelium interactions in situ. Immunopharmacol Immunotoxicol. 2010; 32:402–409. [PubMed: 20095803]
43. Miyama K, Takano K, Atsumi I, Nakagawa H. Identification of C3a and N-truncated C3a as vascular permeability-enhancing factors from the exudate of chronic phase of carrageenan-induced inflammation in rats. Biol Pharm Bull. 2002; 25:648–651. [PubMed: 12033507]
44. Kam WW, Meikle SR, Dunstan CR, Banati RB. The 18 kDa translocator protein (peripheral benzodiazepine receptor) expression in the bone of normal, osteoprotegerin or low calcium diet treated mice. PLoS One. 2012; 7:e30623. [PubMed: 22295097]

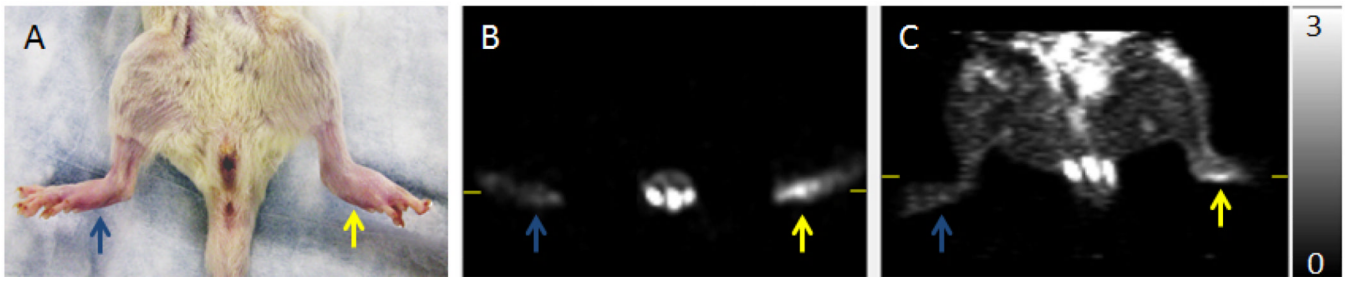

Figure 1.
Photograph (A), as well as axial (B) and coronal (C) [^{11}C]PBR28 microPET images of Carrageenan-treated (yellow arrow) and sham-treated control paws (blue arrow). Carrageenan injection causes acute swelling of the foot as well as increased [^{11}C]PBR28 in the paw.

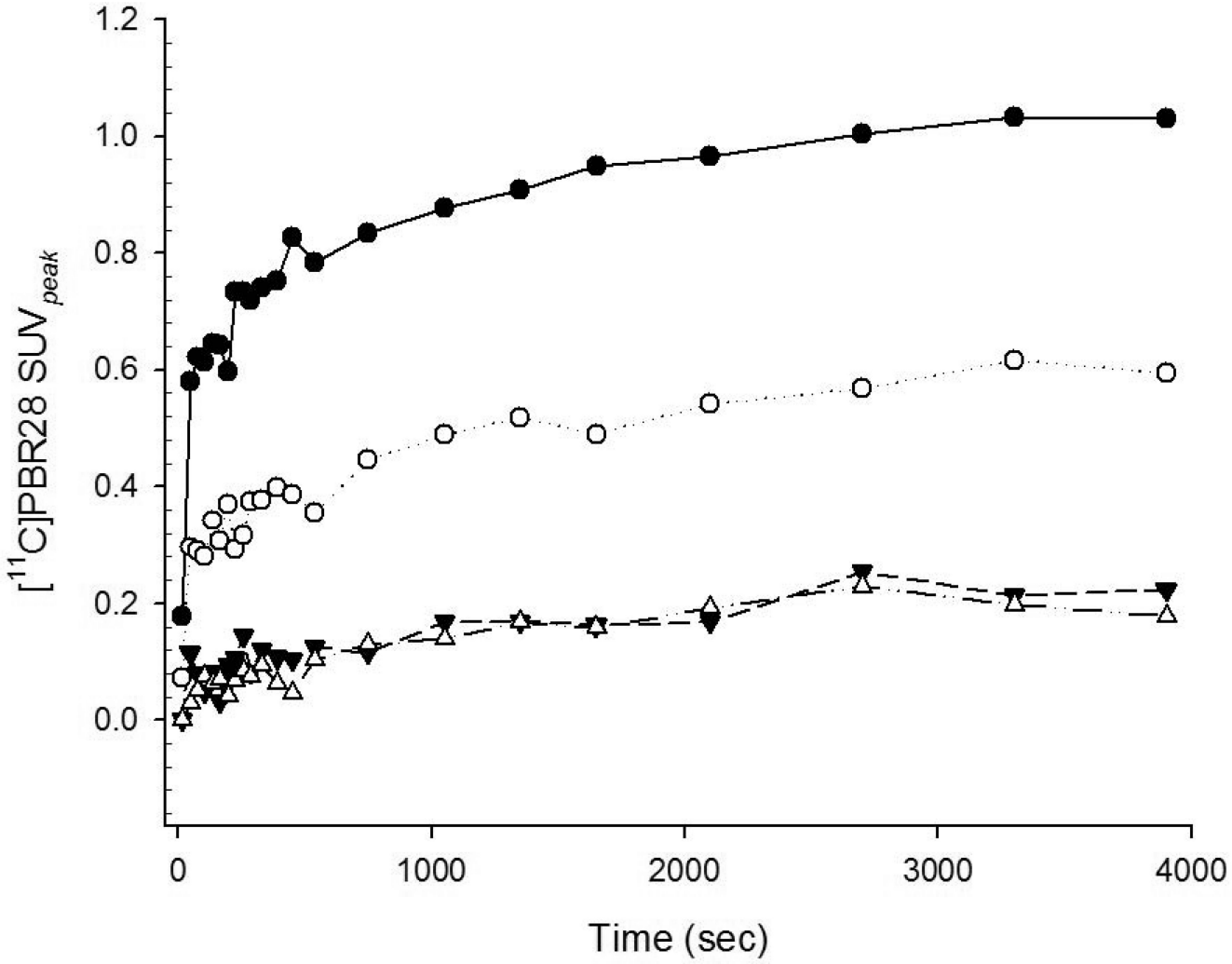

Figure 2.
[^{11}C]PBR28 SUV_{peak} time-activity data show increased tracer uptake of Carrageenan-treated (black circles) compared to sham-treated (white circles) paws with accumulative tracer kinetics. Thigh muscle of the treated (black triangles) and sham-treated (white triangles) are shown for comparison (same case as Figure 1).

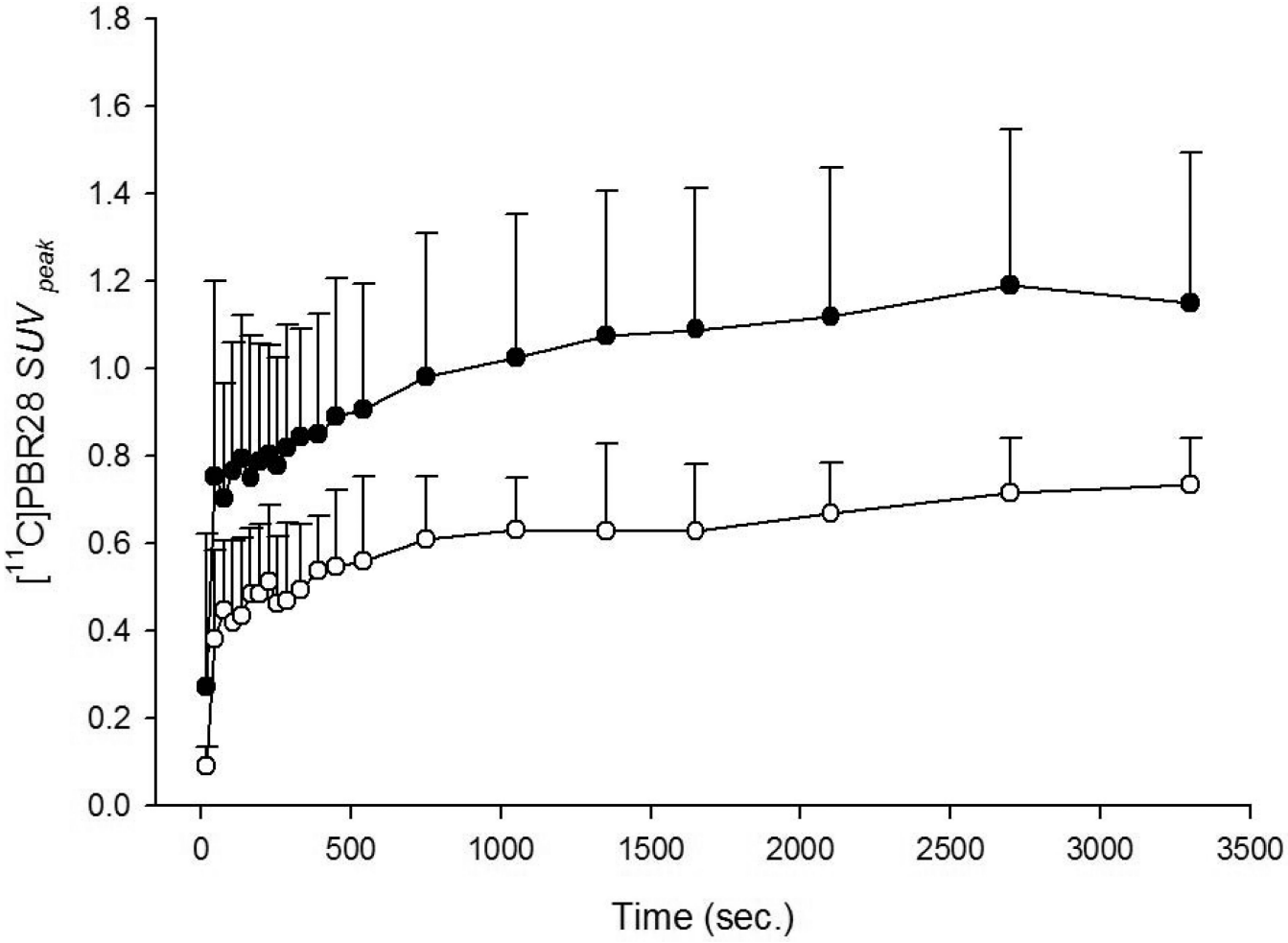

Figure 3.
[^{11}C]PBR28 SUV_{peak} time-activity data of heat-inactivated Mycobacterium butyricum treated (black circles) and sham-treated (white circles) tails display rapid uptake and differential accumulative tracer kinetics favoring treated animals (SUV_{peak} mean ± SD).

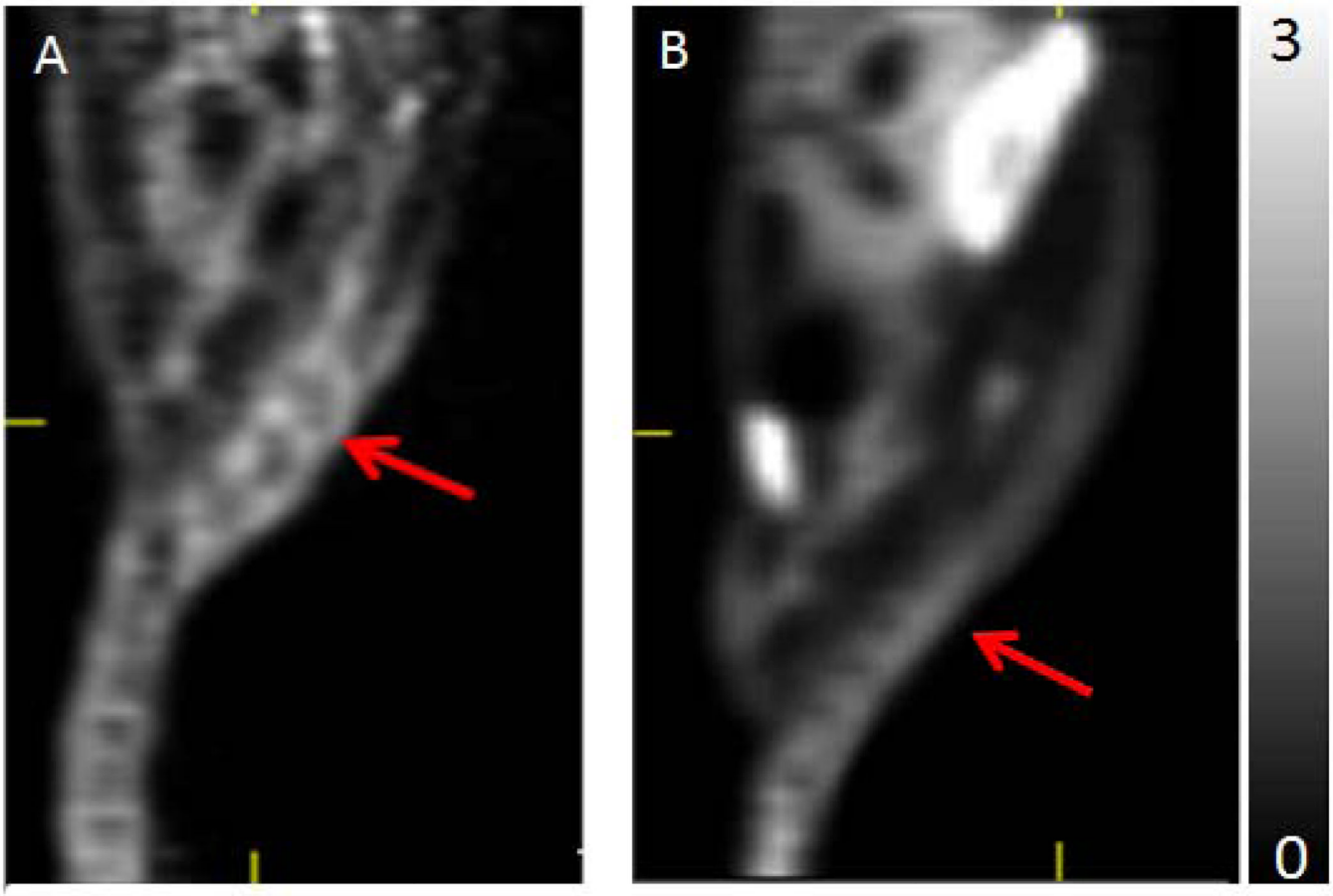

Figure 4.
Sagittal [^{11}C]PBR28 microPET of heat-inactivated Mycobacterium butyricum treated (A) and sham-treated (B) animals. Adjuvant arthritis is identified as increased radiotracer uptake in deformed tail root vertebrae.

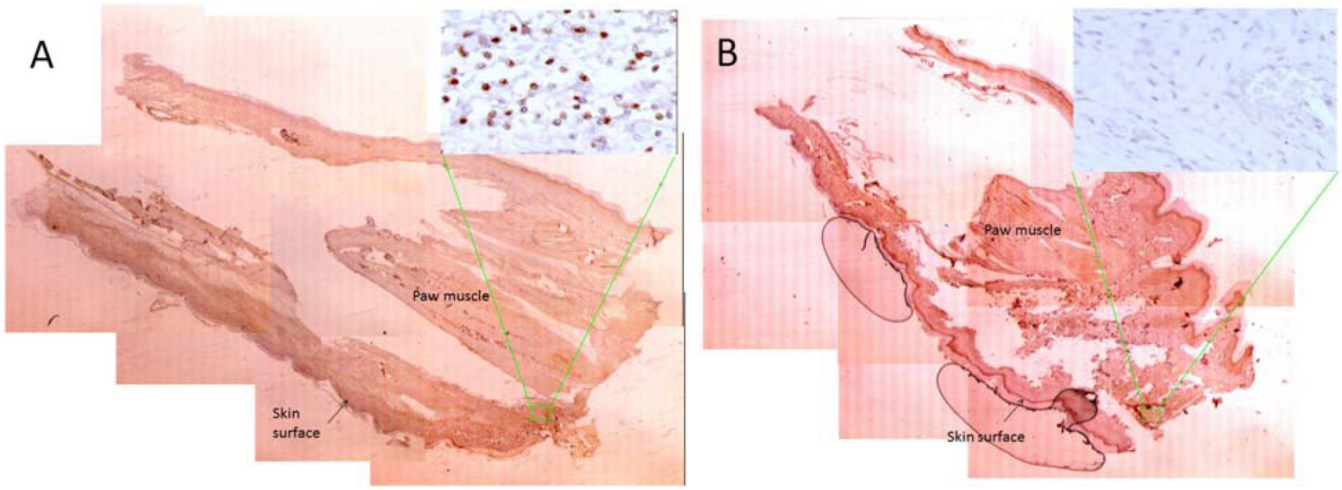

Figure 5.
CD68 immunostaining of Carrageenan-treated (A) and sham-treated control paws (B). Images show an entire paw, delineating the skin surface and central paw muscles, as a mosaic of slides at low power (×1.6) with respective high power detail image (×63) displaying positive CD68 staining in the Carrageenan-treated paw.

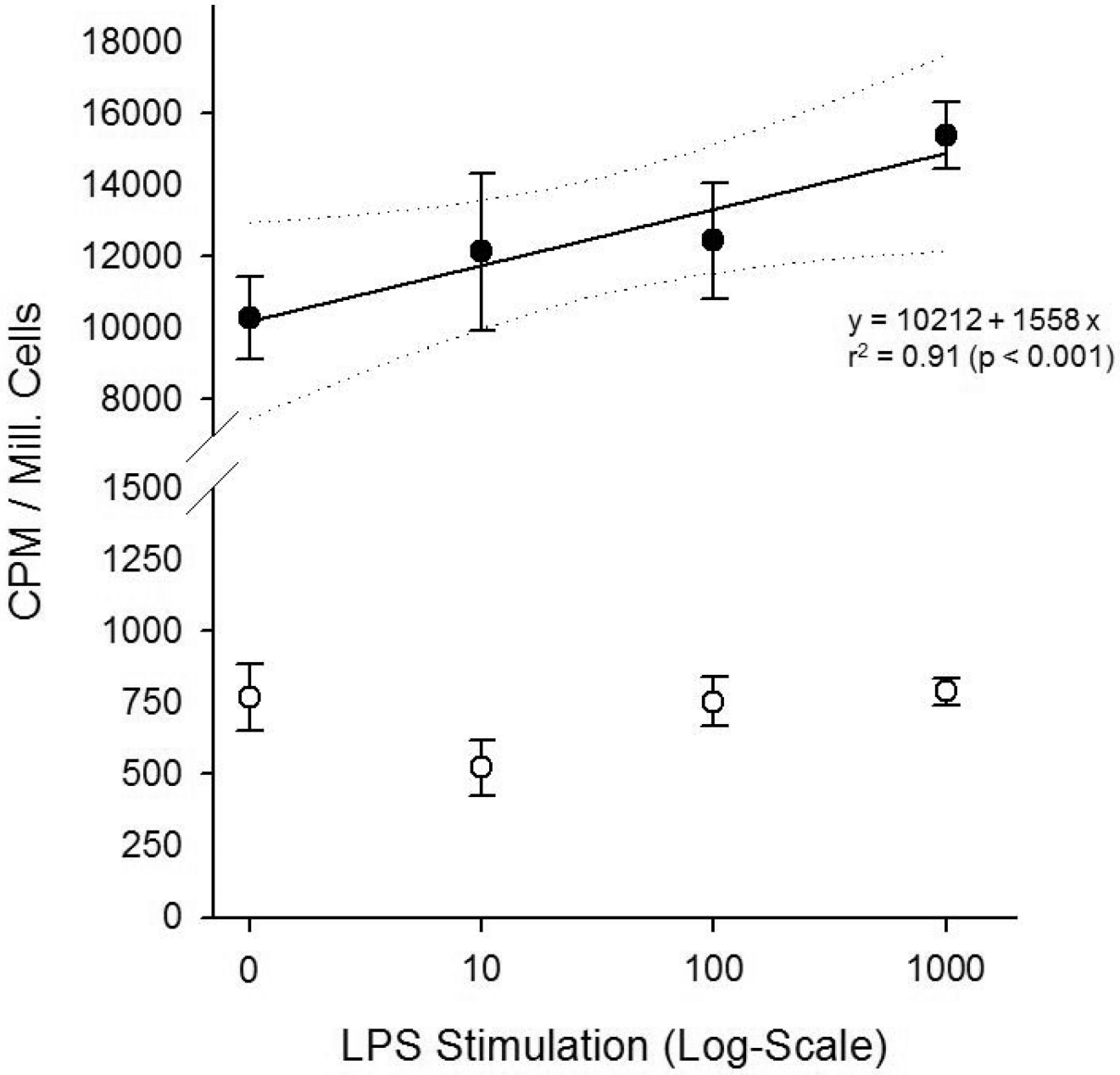

Figure 7.
RAW 264.7 macrophages (black circles) show a dose-dependent increase of [^{11}C]PBR28 with LPS stimulation (x-axis logarithmic scale). Regression analysis results (solid line with dotted 95% confidence intervals) are given. Uptake can be significantly blocked (white circles) by excess non-labeled PBR at any stimulation-level.

TABLE 1

[^{11}C]PBR28 Uptake Measures in Adjuvant-induced Arthritis and Controls

	Adjuvant arthritis (n=8)		Controls (n=4)	
	SUV_{peak}	AUC_{SUV}	SUV_{peak}	AUC_{SUV}
Root of tail	1.27 ± 0.37	3575.9 ± 876.9	0.71 ± 0.11 † *	2081.2 ± 442.4 † ***
Knee joints	1.13 ± 0.41	3438.8 ± 556.4	0.78 ± 0.27 † *	2820.6 ± 427.2 † *
Sacroiliac joints	1.26 ± 0.38	3477.67 ± 1021.9	0.80 ± 0.11 † ***	2380.8 ± 286.1 † ***
Hip joints	1.08 ± 0.32	2832.2 ± 792.3	0.96 ± 1.4 † n.s.	2836.8 ± 410.5 † n.s.
Lumbar spine	1.26 ± 0.47	3285.5 ± 982.2	0.96 ± 1.4 † n.s.	2840.2 ± 347.2 † n.s.
Muscle	0.30 ± 0.35 *** p < 0.001	544.5 ± 252.5 *** p < 0.001	0.26 ± 0.07 † n.s. *** p < 0.001	620.5 ± 191.2 † n.s. *** p < 0.001

† Comparison adjuvant arthritis versus controls

Denotes comparison of any listed region with muscle tissue

Significance level * p < 0.05,

** p < 0.01,

*** p < 0.001;

not significant: n.s.